Am J Physiol Heart Circ Physiol 313: H1063–H1073, 2017.
First published July 28, 2017; doi:10.1152/ajpheart.00651.2016.

RESEARCH ARTICLE | *Vascular Biology and Microcirculation*

Chronic hypertension increases aortic endothelial hydraulic conductivity by upregulating endothelial aquaporin-1 expression

Jimmy Toussaint,[1,4]* Chirag Bharavi Raval,[1,2]* Tieuvi Nguyen,[2]* Hadi Fadaifard,[3] Shripad Joshi,[1] George Wolberg,[3] Steven Quarfordt,[1] Kung-ming Jan,[5] and David S. Rumschitzki[1,5,6]

[1]*Department of Chemical Engineering, City College of the City University of New York, New York, New York;* [2]*Department of Biomedical Engineering, City College of the City University of New York, New York, New York;* [3]*Department of Computer Science, City College of the City University of New York, New York, New York;* [4]*Wellman Center for Photomedicine, Harvard Medical School, Massachusetts General Hospital, Boston, Massachusetts;* [5]*Department of Medicine, Columbia University College of Physicians and Surgeons, New York, New York; and* [6]*Biology (Molecular, Cellular, and Developmental Biology) and Chemistry (Biophysics) Departments, The Graduate School and University Center, City University of New York, New York, New York*

Submitted 28 September 2016; accepted in final form 14 July 2017

Toussaint J, Raval CB, Nguyen T, Fadaifard H, Joshi S, Wolberg G, Quarfordt S, Jan KM, Rumschitzki DS. Chronic hypertension increases aortic endothelial hydraulic conductivity by upregulating endothelial aquaporin-1 expression. *Am J Physiol Heart Circ Physiol* 313: H1063–H1073, 2017. First published July 28, 2017; doi:10.1152/ajpheart.00651.2016.—Numerous studies have examined the role of aquaporins in osmotic water transport in various systems, but virtually none have focused on the role of aquaporin in hydrostatically driven water transport involving mammalian cells save for our laboratory's recent study of aortic endothelial cells. Here, we investigated aquaporin-1 expression and function in the aortic endothelium in two high-renin rat models of hypertension, the spontaneously hypertensive genetically altered Wistar-Kyoto rat variant and Sprague-Dawley rats made hypertensive by two-kidney, one-clip Goldblatt surgery. We measured aquaporin-1 expression in aortic endothelial cells from whole rat aortas by quantitative immunohistochemistry and function by measuring the pressure-driven hydraulic conductivities of excised rat aortas with both intact and denuded endothelia on the same vessel. We used them to calculate the effective intimal hydraulic conductivity, which is a combination of endothelial and subendothelial components. We observed well-correlated enhancements in aquaporin-1 expression and function in both hypertensive rat models as well as in aortas from normotensive rats whose expression was upregulated by 2 h of forskolin treatment. Upregulated aquaporin-1 expression and function may be a response to hypertension that critically determines conduit artery vessel wall viability and long-term susceptibility to atherosclerosis.

NEW & NOTEWORTHY The aortic endothelia of two high-renin hypertensive rat models express greater than two times the aquaporin-1 and, at low pressures, have greater than two times the endothelial hydraulic conductivity of normotensive rats. Data are consistent with theory predicting that higher endothelial aquaporin-1 expression raises the critical pressure for subendothelial intima compression and for artery wall hydraulic conductivity to drop.

hypertension; aquaporin-1; hydraulic conductivity; hydrostatic pressure; aortic endothelial cells; transcellular flow; forskolin

HYPERTENSION INFLUENCES the function of the entire vascular tree, particularly the resistance vessels and conduit arteries preceding them. Prolonged exposure to elevated pressures alters conduit artery (e.g., the aorta) anatomy, biochemistry, and arterial responses to both vasoconstrictive and vasodilatory agonists. These mural changes can contribute to vessel pathology, e.g., atherosclerosis, which can limit perfusion to organs the vessels supply. Changes in renin, angiotensin, endothelial nitric oxide synthase (eNOS), reactive oxygen formation, and prostanoid chemistry have been extensively evaluated in the aortic wall in numerous hypertension models (55). Pathologies induced by these changes cause vessels to activate mechanisms to restore endothelial and vascular quiescence. These processes are less well studied, but Kruppel-like (transcription) factor 2 (KLF2) appears to be an important mediator, inducing a series of genes that regulate eNOS, thrombomodulin, anti-inflammatory mediators, and, relevant to mural water flow, aquaporin-1 (AQP1) (10).

Despite numerous AQP osmotic transport studies in various systems, virtually none have addressed hydrostatic pressure difference (ΔP)-driven/dominant trans-AQP water transport save for our laboratory's recent study of aortic endothelial cells (AECs) (52) and for its postulation in plant root AQPs (57). Nguyen et al. (52) showed that AECs express the ubiquitous membrane protein AQP1. Blockade of AQP1 or reducing AQP1 expression produced corresponding reductions in the hydraulic conductivities (L_p) of AEC monolayers [intrinsic endothelial L_p ($L_{p,e}$)] and vessel wall intimae [L_p of endothelium + subendothelial intima ($L_{p,e+i}$)] subjected to purely hydrostatic ΔP. Parallel ΔP-driven AQP1 and paracellular water flows may be critically important for subendothelial (where atherosclerosis and other pathologies initiate) advective transport and intercellular communication. Both natural increases and interventions to increase (52) AQP1 expression/function may rapidly (minutes to hours) regulate intima $L_{p,e+i}$, which may allow the aortic wall to better respond to ΔP influences and paracrine transport changes. As explained by Nguyen et al. (52) and, in more detail, by Joshi et al. (33), lower AQP1 function lowers $L_{p,e+i}$/reduces transmural flow more at lower than at higher ΔP: at low ΔP, the subendothelial intima (SI) is decompressed,

* J. Toussaint, C. B. Raval, and T. Nguyen contributed equally to this work.
Address for reprint requests and other correspondence: D. S. Rumschitzki, Chemical Engineering Dept., ST319, Convent Ave. at 140th St., New York, NY 10031 (e-mail: david@ccny.cuny.edu).

and the intrinsic endothelial $L_{p,e}$ and medial L_p of denuded vessel: media + internal elastic lamina (IEL) ($L_{p,m+I}$) control transmural water transport. In contrast, higher ΔP compresses the SI so that AECs block IEL fenestrae and reduce flow; SI resistance is far larger than and overshadows any $L_{p,e}$ change. One expects, inversely, increased AQP1 function to decompress the SI at higher ΔP, possibly into the physiological regime, and to increase flow there.

Here, we demonstrate the concomitant upregulation of AQP1, a critical downstream KLF2 signaling target, expression and function for conduit arteries in the AECs of two high-renin rat hypertension models: the spontaneously hypertensive (SHR), genomically altered variant versus its Wistar-Kyoto normotensive (WKY) control and Sprague-Dawley (SD) rats made hypertensive by two-kidney, one-clip (2K1C) Goldblatt (SD-GB) surgery (19) versus normotensive sham or no-operation SD rats. We also compare 2-h forskolin (FSK; a direct cAMP upregulator)-stimulated AQP1 upregulation in (normal renin) normotensive SD rat aortas. We measured AQP1 expression in AECs from whole rat aortas by quantitative immunohistochemistry (QIH) rather than by Western blots, also an antibody method, since the former fixes endothelial cells (ECs) in situ, whereas Western blots require processing including vessel denudation and EC-smooth muscle cell (SMC) separation; EC AQP1 levels can change during this time (5, 56, 77). Careful QIH also allows some assessment of regional variation in AQP1 expression, whereas Western blots (~10^6 ECs) require multiple rat (~10^5 ECs per) thoracic aortas per run. We assess function by measuring the L_p of intact excised aortas at baseline, after chemical (enhancement for FSK-treated aortas and) blocking of AQP1 (both L_p of the intact vessel ($L_{p,t}$)], and again after endothelial denudation ($L_{p,m+I}$), all on the same vessel at the same series of ΔP values. We measure L_p via ΔP rather than by osmotic swelling since ΔP is far larger than osmotic differences in arteries. A mass transfer theory (data not shown) shows negligible change in this ordering in hypertension. From these data, we calculated the apparent SI + endothelial hydraulic conductivities, $L_{p,e+i}$, for each rat cohort and correlated L_p results with AQP1 expression data. We used rats with AQP1 blocking rather than knockout mice and aortas rather than smaller resistance vessels because the L_p measurement technique requires a minimum transwall flow rate, proportional to vessel surface area, for accuracy and an acceptable signal-to-noise ratio (52). AQP1 knockout mice have compensatory mechanisms and suffer pathologies, including microcardia, reduced stroke volume, thin vessels, polyuria, and hypotension, despite impaired nitric oxide (NO)-induced vessel relaxation (24, 47). Rats, normally resistant, can become atherosclerotic with feeding (72, 73). A comparison study by Nguyen et al. (52) of anti-AQP1 siRNA and far easier and faster $HgCl_2$ AQP1 blocking suggests that potential $HgCl_2$ nonspecificity is not a problem here. Enhanced AQP1 expression/function may critically determine conduit artery wall viability and atherosclerotic susceptibility.

MATERIALS AND METHODS

All animal procedures were City College of the City University of New York Institutional Animal Care and Use Committee approved. All rats were obtained from Taconic Biosciences.

Hydraulic Conductivity

Nguyen et al. (52) and Shou et al. (63) have previously described the surgery and L_p measurement procedures with exhaustive technique and toxicity controls. Briefly, we cannulated the aorta and connected it to a fluid reservoir containing 4% (wt/vol) BSA in PBS with 10^{-3} M $NaNO_3$ and 0.03% trypan blue (vital stain and leak reporter) followed by a precision glass tube (into which one can introduce a bubble to measure the flow rate) and then a constant pressure reservoir so as to preserve the endothelium intact when stopping the heart. We excised and placed the thoracic aorta in a petri dish with the same solution minus trypan blue. A sphygmomanometer was used to adjust the reservoir pressure to control transmural ΔP. At each ΔP, we measured vessel dimensions and steady-state transmural flow and calculated L_p. We used physiologically relevant ΔP values, i.e., in the normal range for the rat in question: 60–140 mmHg (non-SHR), 100–180 mmHg (SHR), and 75 and 120 mmHg for the FSK experiments.

For each SHR and WKY aorta, we measured $L_{p,t}$ at five ΔP values, mechanically denuded the endothelia (52, 63, 69), and remeasured L_p at the same ΔP values on the same vessel. For SD/SD-GBs, we did three or four sets of measurements on each vessel (52, 63). For FSK-treated rats, before (or on some rats, instead of) $HgCl_2$ treatment, we flushed with 10 μM FSK (dissolved in 0.1 wt% DMSO in PBS) for 2 h at a 5-mmHg driving pressure difference and measured L_p at the same ΔP values. All L_p measurements were done on each aorta. Intima $L_{p,e+i}$ follows from the addition of specific resistances ($1/L_p$) of vessel layers in series (69):

$$\frac{1}{L_{p,t}} = \frac{1}{L_{p,e+i}} + \frac{1}{L_{p,m+I}} \quad (1)$$

Twelve-week-old SHRs had a systolic blood pressure (BP) of >150 mmHg for ~5 wk. To compare with SHRs, we maintained 2K1C rats at an average systolic BP of >150 mmHg for 5 wk before L_p measurement.

2K1C GB Surgery

We secured a 0.2-μm-internal diameter silver clip around the isolated right renal artery of restrained 5-wk-old anesthetized healthy male 140- to 150-g SD rats kept at 37°C (49). Sham operations were performed in an identical fashion absent clips.

Blood Pressure

BP was measured using a noninvasive BP tail-cuff system attached to a PowerLab module (AD Instruments, Colorado Springs, CO) on rats warmed to ~40°C until multiple reproducible readings resulted. Statistics were performed on these multiple repeated measurements.

Perfusion Fixation, Vessel Harvesting, and Immunohistochemistry

The left femoral vein was cannulated with PE-10 tubing attached to two syringes, one syringe with excess pentobarbital sodium and one syringe with 0.3 ml heparin (5,000 USP U/ml, China Chemical & Pharmaceutical, Taipei, Republic of China). The carotid artery was cannulated and connected to two pressurized syringes: one syringe with 0.3 ml heparin-60 ml PBS and the other syringe with Accustain Bouin's fixative (Sigma Chemical, St. Louis, MO). The trachea was intubated and mechanically ventilated. The rat was perfused through the femoral vein with the heparin and then an overdose of pentobarbital sodium to stop the heart. The carotid artery was perfused with heparin-PBS at 70 mmHg until the efflux from the severed right femoral artery appeared clear and then switched to Bouin's solution at the same pressure with femoral exit. The aorta was removed and placed in Bouin's fixative for 1 h, the connective tissue and adventitia were carefully removed with fine forceps under a dissecting microscope, and the aorta was sectioned into several segments. Segments

were washed in 70% alcohol plus several drops of NH_4OH until all yellow disappeared, placed in 30% sucrose overnight at 4°C, and embedded in Tissue-Tek optimal cutting temperature compound (Sakura Finetek, Torrance, CA). Ten-micrometer-thick cryostat (Thermo Scientific Microm HM 560 Cryostat) sections were collected on Superfrost Plus slides (Fisher Scientific, Pittsburgh, PA) and stained with hematoxylin, Gill no. 2 (Sigma), exactly as previously described by Presnell and Schreibman (58).

To restrict the elastin's significant broad-spectrum autofluorescence to the red, we incubated sections in 0.5% Pontamine Sky Blue 6BX (Alfa Aesar, Haverhill, MA) for 5 min and washed them in PBS for 5 min. For immunohistochemistry, we incubated the slides in blocking solution (3% goat serum, 0.3% Triton X-100, 20 mM sodium phosphate, 0.9 mM NaCl, and 0.05% saponin) to minimize nonspecific staining for 30 min, washed them three times in PBS, and exposed them to rabbit anti-rat AQP1 antiserum (AQP11-A, Alpha Diagnostic) diluted 1:500 (2 μg/ml) in PBS plus 3% goat serum and 0.2% BSA (Sigma) in PBS for 18–24 h. Slides were washed three times in PBS, incubated with Alexa fluor 488-conjugated goat anti-rabbit IgG (Molecular Probes, Carlsbad, CA) at 1:50 dilution in PBS for 90 min at room temperature, washed three times in PBS, and mounted with Vectashield mounting media for fluorescence (Vector Laboratories, Burlingame, CA). Coverslips were secured with clear nail polish, kept in the dark to prevent damage to Alexa fluor 488, and viewed and captured using a Leica TCS SP2 acoustooptical beam splitter (AOBS) confocal microscope.

Immunohistochemistry Control Studies

We performed a no-primary antibody and a small-peptide control. For the latter, excess rat AQP1 control/blocking peptide (AQP11-P, Alpha Diagnostics) was incubated in primary antiboday (AQP1-A, Alpha Diagnostics, 1:50) for 90 min at room temperature and then used in place of the primary antibody.

Confocal Microscopy and Image Analysis

Quantitative fluorescence: laser power meter. We viewed samples on a Leica TCS SP2 AOBS confocal microscope. Before and during every confocal image acquisition set, we calibrated the microscope's laser intensity and maintained the same settings so that each sample received the same type and level of laser power for the same amount of time. This allowed quantitative comparison of different samples.

Internal standards. We compared AQP1 expression between vessels using QIH. Aside from keeping samples in the dark until viewed and exposing them to the same amount of light, we checked that the integrated Alexa fluor 488 fluorescence was proportional to the AQP1 amount. To test the main potential source of nonlinearity, the fluorophore number per secondary antibody, we calibrated the experimental integrated Alexa fluor 488 fluorescent intensity with internal standards. We prepared samples exactly as above except that we applied several known concentrations (0–0.1 mg/ml) of the secondary antibody-PBS to tissue-containing slides. We proceeded exactly as with all other samples using the same settings and 488-nm argon laser. A plot (not shown) showed excellent proportionality of average integrated intensity/rat AEC volume (or area) versus secondary antibody concentration (mg/ml).

Custom software. The confocal microscope yields a *z*-stack of 50 or 20 serial two-dimensional sections. We wrote a custom code to integrate the green intensity in the AECs per unit AEC volume or surface area for slices from both the internal standards and the experiments. With user guidance, active contours or snakes (35) tightly outline and enclose the green Alexa fluor 488-fluorescing endothelial region beyond the IEL in each of the stack's aortic sections. Figure 1*E* of Nguyen et al. (52) shows this outline for the overlay of all 50 images of a stack. The program calculates the perimeter and enclosed area and integrates these and the green intensity inside the contour with Simpson's rule to find the EC surface area, volume, and total green fluorescence for the stack. We examined eight regions from each aorta to get a representative value for that vessel.

Statistics

Paired Student's *t*-tests compared mean integrated Alexa fluor 488 intensity per unit volume or surface area for different treated and control rats. One-way ANOVA compared differences among all the means of a rat group type ($P < 0.05$) followed by post hoc Tukey analysis as the criterion for statistical significance. Values are means ± SE except when standard deviation is explicitly indicated.

RESULTS

Male 2K1C-GB (surgically constricted renal artery) SD rats ($n = 5$) became fully hypertensive (systolic BP of greater than ~200 mmHg) ~5 wk postsurgery and remained hypertensive until death (Table 1). Sham ($n = 2$) and no-operation ($n = 3$) control rats remained stable (~110–120 mmHg) and were pooled. Intergroup differences became significant ($P < 0.05$) after 5 wk.

Figure 1 shows high-magnification confocal images of aortic endothelia/proximal media from control rats (Fig. 1, *A–C*) [no-operation SD (Fig. 1*A*), WKY (Fig. 1*B*), and vehicle-treated SD (Fig. 1*C*)] corresponding to the SD-GB (Fig. 1*D*), SHR (Fig. 1*E*), and SD-FSK-treated (Fig. 1*F*) rats of interest. Each panel overlays 50 (Fig. 1, *A*, *B*, *D*, and *E*) or 20 (Fig. 1, *C* and *F*) serial confocal sections (which introduces blurriness) to yield summed intensities across the sample (all cases: 10 μm total). Images show the (black) lumen, green AQP1 in adjacent ECs, red autofluorescent IEL layer, and well-known (62) medial SMC green AQP1. EC green staining was far less intense in normotensive (Fig. 1, *A* and *B*) than in the corresponding hypertensive rats (Fig. 1, *D* and *E*) and in control (Fig. 1*C*) than in FSK-treated rats (Fig. 1*F*). A reciprocal relationship was obtained for EC and SMC AQP1 staining in control (Fig. 1, *A–C*) versus hypertensive and FSK-treated aortas (Fig. 1, *D–F*).

Figure 2 shows the AQP1 amount/EC volume from Fig. 1 for hypertensive/normotensive (Fig. 2*A*) and SD-DMSO/SD-FSK rats (Fig. 2*B*). In SD-DMSO rats, only 0.1 wt% DMSO was needed to dissolve FSK. SEs expressed aortic region of

Table 1. *Rat systolic blood pressure versus time after SD-GB surgery or after sham operation/no operation*

Rats	*Day 0*	*Day 7*	*Day 14*	*Day 21*	*Day 28*	*Day 35**	*Day 42**	*Day 49*
SD-control	113 ± 6.0/4.2	121 ± 2.9/2.1	109 ± 7.3/5.2	117 ± 19.5/11.2	122 ± 3.0/1.5	118 ± 0.9/0.6	104 ± 4.0/2.9	
SD-GB	112 ± 6.0/4.2	115 ± 10.5/3.0	147 ± 10.1/3.4	144 ± 16.7/9.7	155 ± 27.1/13.6	194 ± 16.4/9.5	203 ± 29.3/14.7	184 ± 24.8/12.4

Values are means ± standard deviation/standard error and are in mmHg. Systolic blood pressure (BP) versus time after two-kidney one-clip Goldblatt (GB) surgery ($n = 5$) or after sham surgery ($n = 3$)/no operation ($n = 2$) for male Sprague-Dawley (SD) rats are shown; control pools the latter two groups. Sham SD rat BP remained stable at ~110–120 mmHg; SD-GB BP rose over ~5 wk to ~200 mmHg and remained there for >2 wk until death. *Times at which differences between curves were significant.

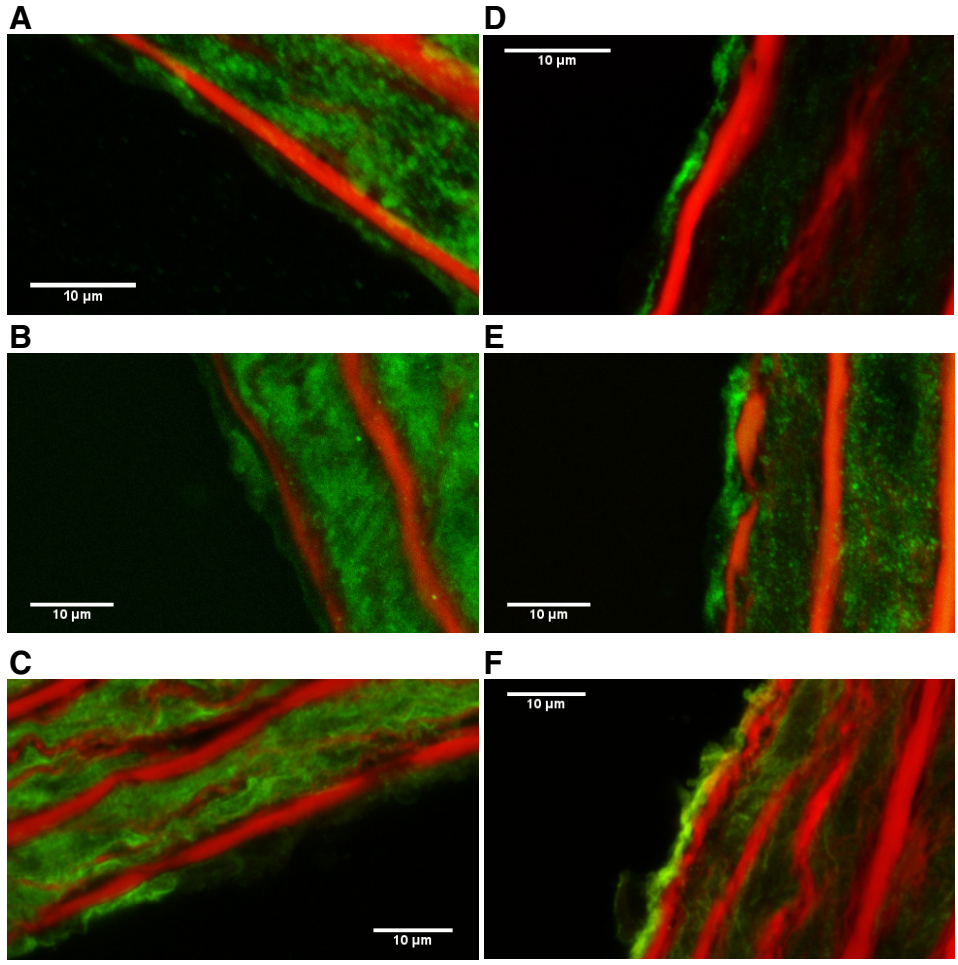

Fig. 1. Aortic wall aquaporin 1 (AQP1) expression for experimental models (*D*−*F*) and their respective controls (*A*−*C*). Overlays (which induce blurriness) of 50 (*A*, *B*, *D*, and *E*) or 20 (*C* and *F*) serial confocal sections (all cases: 10 μm total) of an aorta from a male Sprague-Dawley (SD) rat (*A*), Wistar-Kyoto (WKY) rat (*B*), vehicle-treated SD rat (*C*), SD rat subjected to Goldblatt surgery (SD-GB; *D*), spontaneously hypertensive rat (SHR; *E*), and SD rat treated with forkolin (FSK; *F*). The endothelial green AQP1 region is adjacent to the black lumen followed by the inner elastic lamina (IEL; red) and alternating green [smooth muscle cell (SMC) AQP1] and red (elastin) medial regions. Endothelial AQP1 staining was more intense in hypertensive (*D* and *E*) and FSK-treated (*F*) aortas than in their controls (*A*–*C*).

interest (ROI) variability. SHR (SD-GB) aortic ECs of $n = 35$ ($n = 31$) ROIs expressed ~2.5 (>2) times the AQP1 of normotensive WKY ECs (sham or no-operation SD rats) [$n = 31$ ($n = 30$) ROIs, $P << 0.01$ ($P < 0.05$); Fig. 2*A*]. Sham and no-operation SD aortic EC AQP1 expressions were identical and only slightly higher ($P > 0.05$) than those of normotensive WKY rats. AQP1 upregulation in genetically and surgically induced hypertension models was consistent. SD-FSK aortic ECs ($n = 19$ ROIs) expressed >3 times ($P < <0.01$) the AQP1 of SD-DMSO rat aortas ($n = 15$ ROIs; Fig. 2*B*). FSK directly upregulates adenyl cyclase and may increase AQP1 by a cAMP upregulation pathway. Thus, both elevated BP and FSK-enhanced cAMP levels display appreciable EC AQP1 upregulation.

We turn now to function. Figure 3 shows that denuded vessel (medial SMCs, matrix, and elastic layers) $L_{p,m+I}$ was ΔP insensitive for each rat model (ANOVA, $P > 0.05$), as previously described (2, 52, 63, 69). Normotensive and hypertensive $L_{p,m+I}$ values each agreed ($P > 0.05$) for both rat strains. FSK-treated rat $L_{p,m+I}$ lay on the normotensive curve at both ΔP values evaluated. Hypertensive aortic $L_{p,m+I}$ was far lower ($P << 0.01$) than its control normotensive $L_{p,m+I}$ for both strains. Intact $L_{p,t}$ was consistently higher for WKY rats than for SHRs (ANOVA and post hoc Tukey test, $P < 0.05$; Fig. 4*A*) at the three common ΔP values and for SD-GB than for SD rats (; $P << 0.01$; Fig. 5), which reflects the well-known media thickening/remodeling that prolonged hypertension induces (22).

Consistent with a prior SD rat Lp study (63), WKY intact (total) $L_{p,t}$ (Fig. 4*A*) and intimal (endothelial + subendothelial) $L_{p,e+i}$ (Fig. 4*B*) were high at 60 mmHg, dropped (~15 and 40% for $L_{p,t}$ and $L_{p,e+i}$, respectively) by ~100 mmHg, and were flat at 140 mmHg. In SD rats (Fig. 5*A*) (52), this $L_{p,t}$ drop reflects SI compression under ΔP, which increases wall flow resistance, $1/L_{p,t}$, by causing ECs to block IEL fenestrae (29, 30). (The SHR vs. WKY $L_{p,t}$ comparison above is in the ΔP overlap region where the SI is likely fully compressed for both rat species.) Since both intact and denuded L_p values were measured on each rat, one can calculate $L_{p,e+i}$ for each rat at each ΔP from *Eq. 1*. Clearly (Fig. 4*A*), the SHR intact and denuded curves were much closer together, i.e., had far lower flow resistant (quantified in Fig. 4*B*) endothelia, than the WKY curves. SHR $L_{p,e+i}$ is ~2 times the WKY $L_{p,e+i}$ at ΔP values where both were measured and where WKY $L_{p,t}$ has leveled off [i.e., for pooled $\Delta P = 100$, 120, and 140 mmHg values ($P < 0.02$) or independently compared $\Delta P = 100$ and 120 mmHg values ($P < 0.02$)]. SHRs' thickened media/lower $L_{p,m+I}$ gives them a higher overall flow resistance, $1/L_{p,t}$, than WKY rats despite SHRs' significantly higher $L_{p,e+i}$. The more facile transintimal and more difficult transmedial water flow point to SI thickening, i.e., less SHR fenestral blocking.

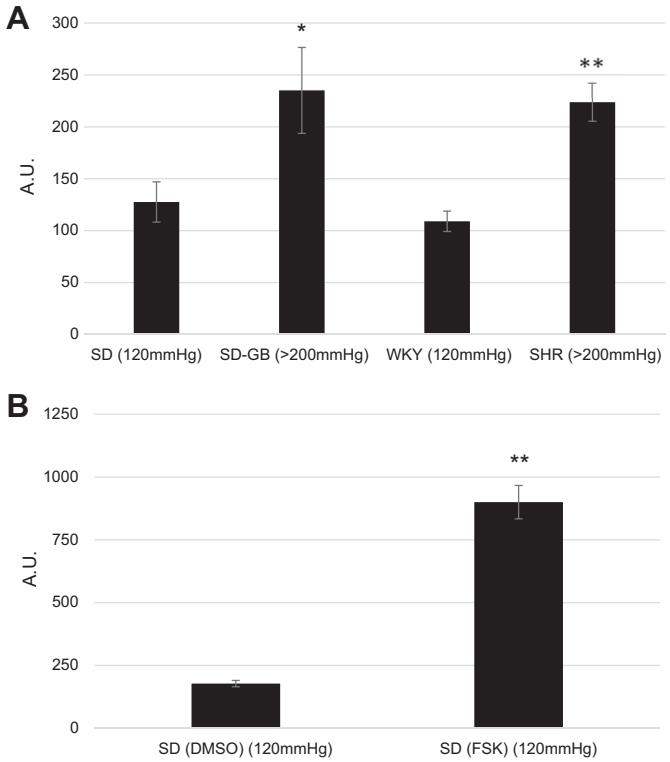

Fig. 2. Quantified aquaporin 1 (AQP1) fluorescent intensity ±SE of rat aortic endothelia comparing aortas of male normotensive Wister-Kyoto (WKY) rats versus their spontaneously hypertensive variant (SHR) and normotensive Sprague-Dawley (SD) versus surgically induced hypertensive SD (SD-GB) rats ($n \geq 29$ regions of interest; *A*) as well as control versus forskolin (FSK)-treated SD rats ($n \geq 15$ regions of interest; *B*). In both hypertensive models, elevated blood pressure correlated with >2-fold AQP1 expression of the corresponding normotensive rat aortas (SD-GB vs. SD, $*P < 0.02$; SHR vs. WKY, $**P << 0.01$). FSK elevated rat aortic endothelial cell AQP1 expression in whole rat aortas ex vivo ($**P << 0.01$). Only vessels in *B* were perfused with (FSK/DMSO or DMSO) solution ex vivo before fixation/immunohistochemistry, and, more importantly, laser light illuminated fewer (20 vs. 50) optical sections in *B* than in *A*; thus, the different scales in *A* and *B*. Each bar contains regions of interest from at least 2–3 rats. A.U., arbitrary units.

SD-GB rats, with wild-type genomes, yielded similar intimal and medial water flow changes to SHRs. Since the medial is the dominant SD-GB resistance, their $L_{p,t}$ values were lower than SD $L_{p,t}$ values at all ΔP values (Fig. 5, *A* and *B*). Again, the hypertensive SD-GB $L_{p,t}$ and $L_{p,m+I}$ curves were much closer together (much less resistant endothelia/far larger $L_{p,e+i}$) than for normotensive SD rats. [*P* values comparing SD/SD-GB $L_{p,t}$ differences were as follows: 0.016 (60 mmHg), 0.003 (100 mmHg), and 0.006 (140 mmHg); *P* values on inverses needed to calculate $L_{p,e+i}$ were not enlightening since inverses magnify small differences.]

Both hypertensive and normotensive SD rat aortic $L_{p,t}$ values dropped from 60 to 100 mmHg (ANOVA and post hoc Tukey test showed that the only significant difference was $L_{p,t}$ for 60 vs. 100 and 140 mmHg for SD rats; this distinction was only suggestive for SD-GB rats), but denuded $L_{p,m+I}$ was ΔP independent (Fig. 5, *A* and *B*). As in normotensive WKY and SD rats, the higher ΔP-compressed SD-GB SI contributed a larger fraction of total wall flow resistance than the lower ΔP-uncompressed SI. Figure 5*C* shows $L_{p,e+i}$ (*Eq. 1*) for the rats shown in Fig. 5, *A* and *B*, along with SD-FSK and SD-DMSO rats. For both SD and SD-GB rats, $L_{p,e+i}$ dropped from 60 to 100 mmHg as ΔP compressed the SI, but it dropped far more for hypertensive rats. Similarly, intact SD $L_{p,e+i}$ dropped from 75 to 120 mmHg before FSK treatment (values consistent with the other normotensive SD rats), but the drop was far more pronounced, and similar to SD-GB drops, after FSK treatment; all $L_{p,e+i}$ drops were significant. FSK more than doubled $L_{p,e+i}$ at 75 mmHg but inflicted no apparent change at 120 mmHg. The 60-mmHg SD-GB $L_{p,e+i}$ was only slightly below the 100-mmHg SHR $L_{p,e+i}$ (Fig. 4*B*), but its higher ΔP values were far lower. Both hypertensive SHR (Fig. 4) and SD-GB aortas (Fig. 5) had lower $L_{p,m+I}$ and higher $L_{p,e+i}$ and delayed transmedial and accelerated transintimal water flow than normotensive aortas.

Nguyen et al. (52) showed that AQP blocking with 5 μM $HgCl_2$ is fully reversible and that blocking SMC AQPs causes no measurable $L_{p,m+I}$ change. The post-$HgCl_2$ curves shown in Fig. 5 thus reflect EC AQP1 suppression. The nine L_p values shown in Fig. 5 are at just three ΔP values so that each vessel remains viable for all three L_p sets. Each aorta showed a percent drop with $HgCl_2$ at each ΔP and its mean ± SE (Fig. 6). The drops at 60 mmHg shown in Fig. 5 were statistically different ($P < 0.05$) from those at 100 and 140 mmHg for both SD-GB and SD rats. Unlike unblocked $L_{p,t}$, in both rat cohorts both blocked $L_{p,t}$ values and denuded $L_{p,m+I}$ values were essentially ΔP independent from 60 to 140 mmHg (Fig. 5, *A* and *B*). Denuded $L_{p,m+I}$ values were ~2 times the high-ΔP $L_{p,t}$ for each rat cohort; that is, at maximal SI compression, the endothelium + SI accounted for approximately half the overall aortic wall transmural flow resistance (29, 30).

Joshi et al. (33) extended Huang et al.'s (30) filtration flow theory through an artery wall with a compressible SI by including trans-EC, trans-AQP1 flow. It predicts that an increase/decrease in EC AQP1 shifts to higher/lower ΔP the dynamic regime over which $L_{p,t}$ drops from its low-ΔP to its

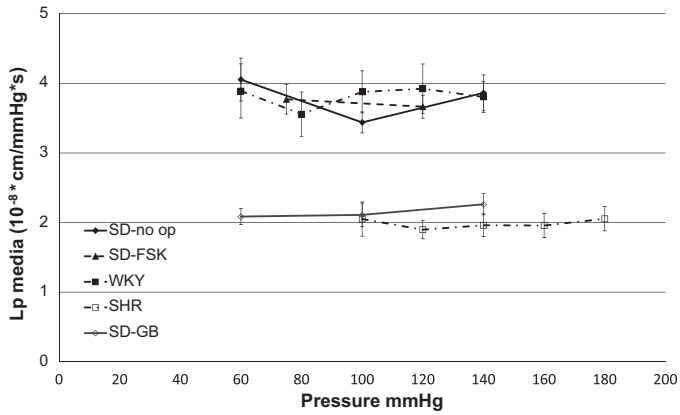

Fig. 3. Medial hydraulic conductivity (L_p) [denuded: media + inner elastic lamina ($L_{p,m+I}$)] ± SE versus transmural pressure for the two normotensive/hypertensive rat models [Wister-Kyoto (WKY)/spontaneously hypertensive rats (SHR), $n = 5/5$; Sprague-Dawley (SD) rats with no-operation (no op)/SD rats subjected to Goldblatt surgery (SD-GB), $n = 6/6$; and (predenudation) forskolin (FSK)-treated rats, $n = 8$]. After denudation, FSK treatment did not change $L_{p,m+I}$ ($n = 2$; not shown). Normotensive and hypertensive $L_{p,m+I}$ are each independent of the transmural pressure difference and rat strain (ANOVA, $P > 0.05$). FSK-treated SD vessel and normotensive $L_{p,m+I}$ values coincide.

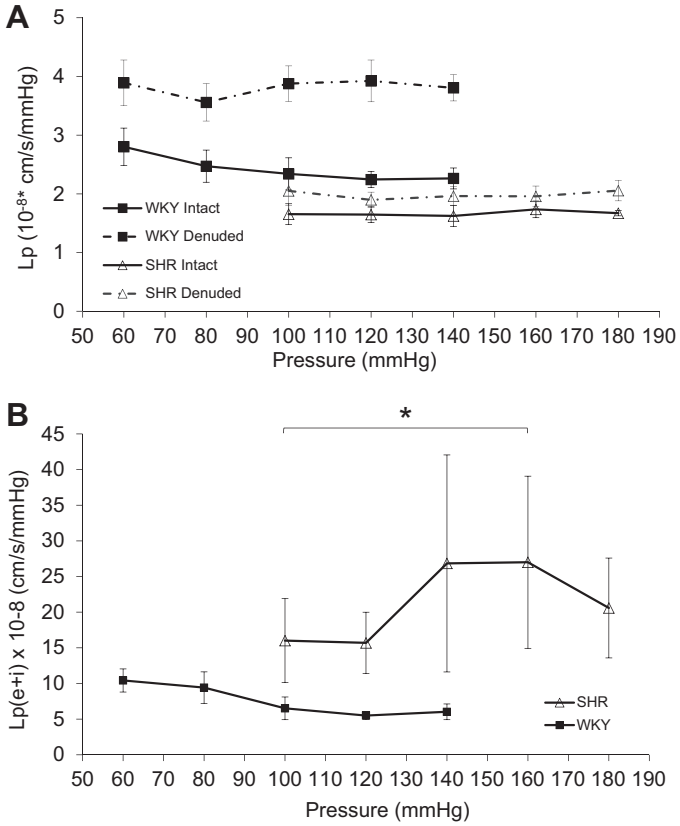

Fig. 4. Spontaneously hypertensive rat (SHR) and normotensive Wistar-Kyoto (WKY) rat aorta hydraulic conductivity (L_p) versus the transmural pressure difference (ΔP) before and after denudation. *A*: intact L_p of the intact vessel ($L_{p,t}$) ± SE and L_p of the denuded (media + inner elastic lamina) ($L_{p,m+I}$) aorta versus ΔP for SHR versus WKY rats ($n = 5$ and 5, respectively), each over its physiological pressure range. WKY and Sprague-Dawley (SD) aortic $L_{p,t}$ values displayed similar trends: high at 60 mmHg, dropping [~15% ($P < 0.01$), less than in SD rats; Fig. 5*B*] by 100 mmHg, and flat to higher ΔP values. Endothelial denudation approximately doubled the high-ΔP WKY $L_{p,t}$ values and rendered $L_{p,m+I}$ ΔP independent. SHR $L_{p,t}$ and $L_{p,m+I}$ curves were both flat at the (higher) ΔP values tested, well beyond ΔP for subendothelial intima (SI) compression (SI cellularity permitting), and far closer together than the WKY curves. This indicates that the SHR endothelium presents a far smaller fraction of total wall flow resistance than that in WKY rats despite SHRs' thickened media and far higher overall flow resistance. *B*: thus, L_p of the endothelium plus SI ($L_{p,e+i}$) is roughly double that of WKY rats. *Significant L_p differences (ANOVA, $P < 0.05$).

high-ΔP plateaus. Figure 7 shows a recalculation of Joshi et al.'s theory using our rats' baseline $L_{p,m+I}$ and untreated $L_{p,t}$ values, which were uniformly a bit lower than Nguyen et al.'s (52) and Tedgui and Lever's (69),[1] while retaining their ΔP value (88 mmHg) for full SI compression. Blockade of AQP1 should have a big effect at 75 mmHg, through which the dynamic range shifts, but a much smaller one (likely within measurement error bars) beyond it at 120 mmHg. The results shown in Fig. 7 demonstrated good consistency between theory and experiment ($L_{p,t}$ from Fig. 5*C*) and predicted ~150% EC AQP1 upregulation with FSK.

Figure 6 shows the percent drops, all significantly nonzero, with $HgCl_2$ in $L_{p,t}$ (Fig. 6, *A* and *C*) and $L_{p,e+i}$ (Fig. 6, *B* and *D*) for SD-GB and SD (Fig. 6, *A* and *B*) and SD-FSK and SD-DMSO rats (Fig. 6, *C* and *D*) from Fig. 5. $HgCl_2$ lowered $L_{p,t}$ versus baseline at each ΔP for all rats, with the largest average drop at 60 mmHg: 31.9 ± 3.7% (SD) and 38.9 ± 5.4% (SD-GB; Fig. 6*A*); it lowered $L_{p,e+i}$ by 58.2 ± 7.6% (SD) and 77.2 ± 6.0% (SD-GB) at 60 mmHg (Fig. 6*B*). Note that despite the different L_p magnitudes in Fig. 5, *A* and *B*, the percent drops with $HgCl_2$ (Fig. 6, *A* and *B*) were nearly the same for SD-GB and SD rats at each ΔP. In contrast, FSK-treated SD rats showed much larger drops at 75 mmHg but the same drops at 120 mmHg as untreated SD rats. The different normotensive percent drops at 60 and 75 mmHg suggest that $L_{p,t}$ and $L_{p,e+i}$ lose much of their sensitivity to AQP1 blocking by ~75–80 mmHg, consistent with approximately fully compressed SIs with or without $HgCl_2$. In contrast, FSK-treated rat aortas had

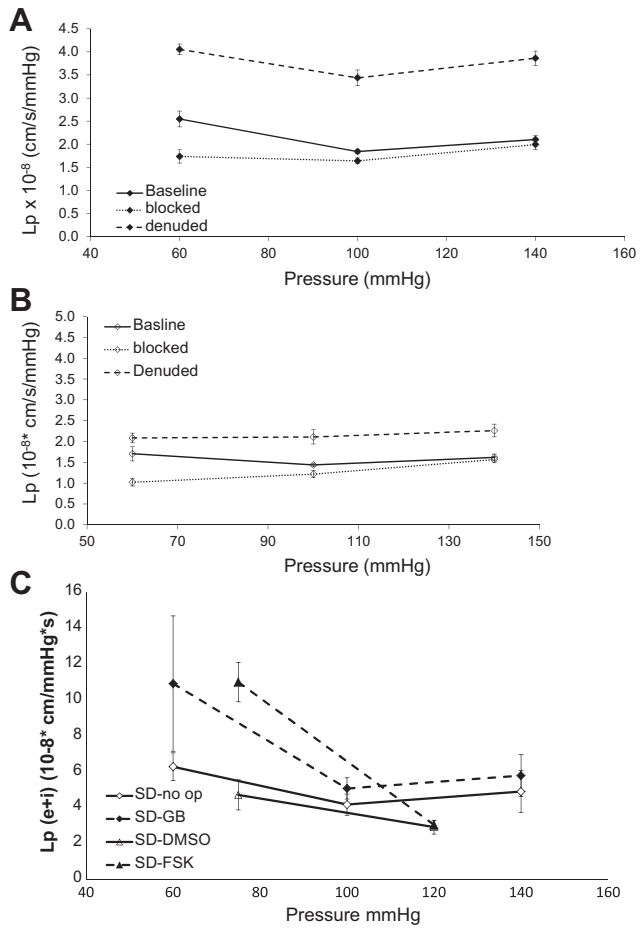

Fig. 5. Baseline, blocked, denuded hydraulic conductivity (L_p) for aortas from normotensive Sprague-Dawley (SD) rats with no operation (no op; *A*) and hypertensive SD rats subjected to Goldblatt surgery (SD-GB; *B*) and L_p of the endothelium plus subendothelial intima ($L_{p,e+i}$) for these and for forskolin (FSK)-treated rats (*C*): L_p of the intact aorta before and after $HgCl_2$ aquaporin 1 blockade and $L_{p,m+I}$ of the denuded vessel (media + inner elastic lamina) after denudation, each at the same three transmural pressure difference values, all on each aorta (*A* and *B*: $n = 6$ and 6, respectively). This allowed $L_{p,e+i}$ (*C*: mean ± SE) calculation (*Eq. 1*) for each vessel. Results in *C* include $L_{p,e+i}$ for FSK versus control treatment. SD-GB L_p values were uniformly lower than normotensive SD aorta L_p values but followed similar trends (see text). Hypertensive SD-GB and FSK-treated aortic $L_{p,e+i}$ values were far higher at low pressure (and similar to SHR $L_{p,e+i}$ values; Fig. 4*B*) but dropped substantially at higher pressures ($n = 8$). Data in *A* and the no-operation curve in *C* are from Nguyen et al. (52).

[1] This absolute variation is normal; trends with treatment are far more aorta independent.

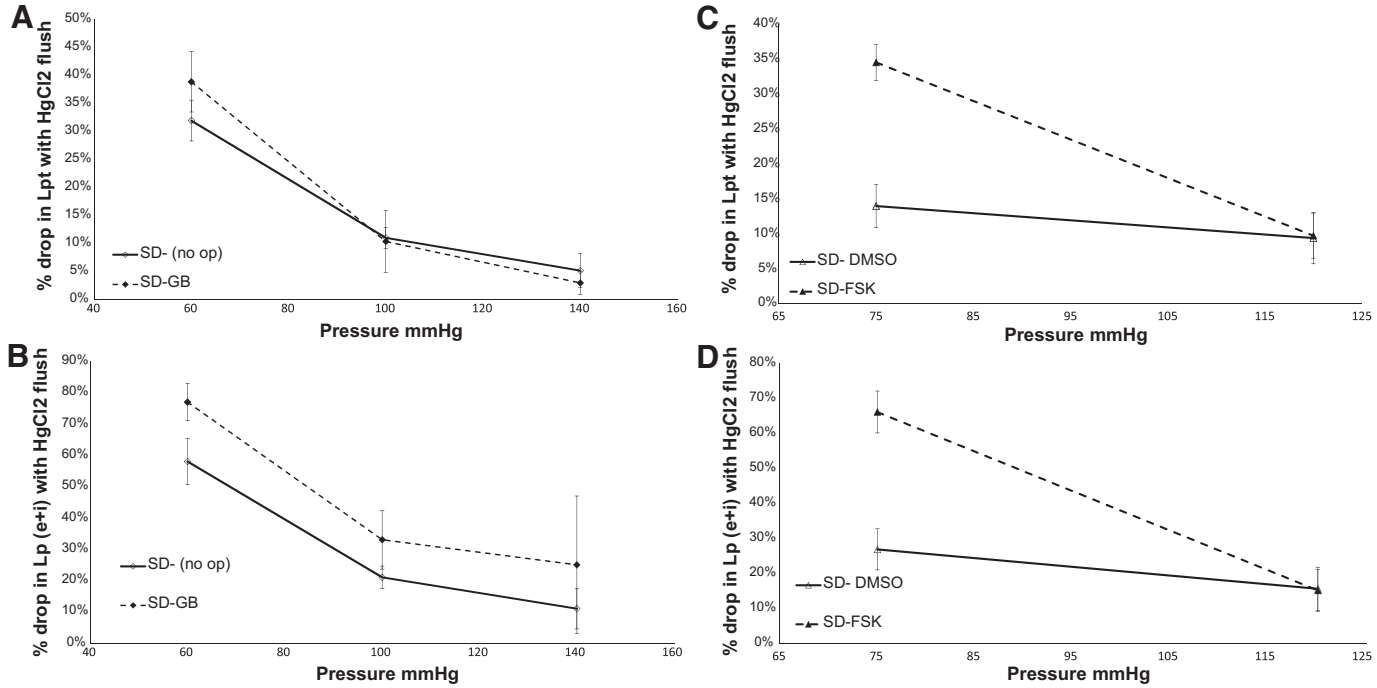

Fig. 6. Percent drops in hydraulic conductivity (L_p) in the intact vessel ($L_{p,t}$) and endothelium + subendothelial intima ($L_{p,e+i}$) by $HgCl_2$ treatment for Sprague-Dawley (SD) rats subjected to Goldblatt surgery (SD-GB) compared with SD rats with no operation (SD no op) (*A* and *B*; $n = 6$) were similar for both cohorts despite different absolute L_p values (Fig. 5). *C* and *D*: values for pre/post-foskolin treatment (FSK) SD rats ($n = 4$). Comparison of low-pressure normotensive $L_{p,t}$ values in *A* and *C* and $L_{p,e+i}$ values in *B* and *D* suggests that both L_p values lose sensitivity to aquaporin 1 blocking (consistent with compressed subendothelial intima with or without $HgCl_2$) by ~75–80 mmHg. In contrast, after FSK-increased aquaporin 1 expression, SD rats retained $HgCl_2$ sensitivity (decompressed subendothelial intima) up to ≥75 but lost it by 120 mmHg (compressed subendothelial intima even without $HgCl_2$).

similar $HgCl_2$-induced drops at 60 and 75 mmHg, consistent with SI decompressed after FSK treatment. At 120 mmHg, both pre- and post-FSK aortas showed little $HgCl_2$ sensitivity, consistent with fully compressed SIs with or without $HgCl_2$. These results suggest that EC AQP1 expression and function modulate the portion of ΔP acting across the endothelium, as in Fig. 7.

DISCUSSION

Both chronic hypertension in either genetically hypertensive SHRs or SD rats made hypertensive by renovascular surgery and 2-h FSK-treated SD rat aortas cause a 2- to 3-fold upregulation in aortic EC AQP1 expression [Figs. 2 and 3; microRNAs may play a role (8, 9)] and a doubling (SD-GB, 75 mmHg; SHR, all ΔP) or tripling (FSK, 75 mmHg) in $L_{p,e+i}$. SHRs also have elevated inner medulla (39) and, at high ΔP, choroid plexus (70) AQP1 expression; in contrast, low-renin hypertensive, antibody-induced anti-thyroglobulin type-1 (Thyr1) glomerulonephritis mice and rats have reduced proximal tubule AQP1 expression (16, 36) as do SD-GBs, at least at 1 wk postsurgery (43). The present quantitatively similar rise in AEC AQP1 expression and function indicates that its enhanced expression alone, rather than chemical modification (unless it affects antibody recognition) or trafficking, could explain the parallel rise in $L_{p,e+i}$ if transendothelial water transport were mostly through AQP1. Since much of this transport is paracellular (33, 52), AQP1 changes and SI compression also contribute (below) to a fuller explanation of these increases. Nevertheless, this parallel rise complements Nguyen et al.'s (52) finding that rat and bovine AECs express AQP1 and reducing functioning AQP1 lowers $L_{p,e+i}$. It supports their conclusion that AQP1 facilitates hydrostatic ΔP-driven trans-EC flow, accounts for a significant fraction of intrinsic aortic endothelial $L_{p,e}$, and impacts $L_{p,e+i}$ via both $L_{p,e}$ and SI compression.

Regional variability (SEs) in ROI AQP1 expression in a single aorta is similar to that between aortas, consistent with known local variation in hemodynamics and atherosclerotic susceptibility (4, 11, 50, 51, 74). We did not systematically attempt to correlate them and avoided branch site ROIs. We focused only on aortas since our L_p study required a minimum vessel size.

High ΔP lowers $L_{p,e+i}$ by compressing the SI and causing ECs to block IEL fenestrae (29, 30). Joshi et al.'s (33) filtration theory predicts that raising/lowering functioning EC AQP1 raises/lowers the critical ΔP that achieves the compressing trans-EC pressure difference (force/area) (33, 52) and thus the dynamic range over which $L_{p,t}$ drops. Nguyen et al.'s (52) data, plotted versus theory given by Joshi et al. (33), are consistent with a decrease in EC AQP1 shifting this critical ΔP and dynamic regime to lower ΔP ($\Delta P << 60$ mmHg). Inversely, in AQP1-upregulated aortas, compression might begin above 75 mmHg. Thus, AQP1 blocking would compress the SI, causing a large $L_{p,t}$ drop at 75 mmHg, but barely change $L_{p,t}$ at 120 mmHg where the SI is already compressed. In fact, FSK nearly triples both EC AQP1 expression (Fig. 2) and $L_{p,e+i}$ at 75 mmHg but leaves $L_{p,e+i}$ unchanged at 120 mmHg (Fig. 5*C*), in agreement with Joshi et al. (Fig. 7) and consistent with FSK raising the critical ΔP from <75 to >75 mmHg. Similarly,

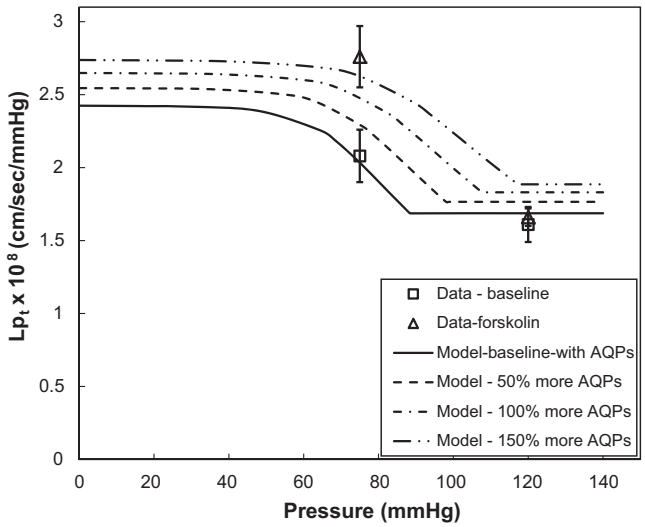

Fig. 7. Comparison of Joshi et al.'s (33) theoretical predictions with the data from the experiment shown in Fig. 5*C* ($n = 8$). Recalculated theory for present baseline hydraulic conductivity (L_p) of the denuded vessel (media + inner elastic lamina) ($L_{p,m+I}$) and untreated L_p of the intact vessel ($L_{p,t}$) values that were uniformly slightly lower than those given by Nguyen et al. (52) while retaining their transmural pressure difference at ~88 mmHg for full subendothelial intima compression gave a subendothelial intima elasticity constant of 29.3 mmHg. It predicted that blockade of aquaporin 1 with $HgCl_2$ would have a large effect at 75 mmHg versus a likely unmeasurable effect at 120 mmHg, which the data show. These data and those of Nguyen et al. support Joshi et al.'s prediction that the dynamic regime of $L_{p,t}$ goes up (down) with more (less) functioning endothelial cell aquaporin 1 channels.

SD-GB $L_{p,e+i}$ seems to[2] far exceed SD $L_{p,e+i}$ at 60 mmHg but not at 100 and 140 mmHg (Fig. 5*C*). Taken together, these data support Joshi et al.'s theory that raising/lowering functioning EC AQP1 numbers raises/lowers the critical ΔP needed for SI compression and thus $L_{p,t}$'s dynamic regime. On the other hand, SHR SI may have lower SI compressibility or not compress, possibly because of differences in anatomy (e.g., SI cellularity) or extracellular matrix chemistry (23). Unique among the high-AEC AQP1 rats studied, SHRs show flat $L_{p,t}$ and flat and elevated $L_{p,e+i}$ for ΔP studied ($100 < \Delta P < 180$ mmHg); the lack of low-ΔP SHR data precludes a direct check if $L_{p,t}$ rises at low ΔP. However, SHR $L_{p,e+i}$ ($1.6–2.7 \times 10^{-7}$ cm·s^{-1}·mmHg^{-1}) at all ΔP values exceeds literature values [~$(0.7–1.6) \times 10^{-7}$ cm·s^{-1}·mmHg^{-1} (52, 63, 71)] for intrinsic endothelial $L_{p,e}$ of normotensive aortas and $L_{p,e+i}$ of FSK-treated, AQP1-upregulated, likely SI-decompressed SD aortas at 75 mmHg (Fig. 5*C*). Note that normotensive $L_{p,t}(\Delta P)$ and $L_{p,m+I}(\Delta P)$ are consistent for SD and WKY rats (Figs. 4*A* and 5*A*).

Elevated pulse (systolic-diastolic) pressures in hypertension induce changes in aortic wall biomechanics because of larger wall distensions. Mechanical factors including stretch, strain, shear, and ΔP contribute to vascular pathophysiology. ΔP-induced stretch expands the aortic lumen, but $L_{p,t}$ remains flat above 100 mmHg (2, 3, 63). For 120-, 180-, and 240-mmHg intraluminal pressures, Giannakoulas et al. (18) computed peak von Mises wall stresses (a mixture of normal and tangential stresses) of 22.5, 32.0, and 40.6 N/cm^2 and maximum wall displacements of 0.44, 0.59, and 0.72 mm, respectively. BP rise affects all stresses [e.g., reduces carotid artery wall shear stress (40)], which affects the EC cytoskeleton and adherens junctions and, in turn, can influence AQP1 expression and trafficking. It can cause alteration of arterial gene expression and protein production (here), increased $L_{p,e}$, and, over long times, wall remodeling and sometimes atherosclerosis (27). Rapidly elevated ΔP, stretch, and EC AQP1 expression increase transendothelial water flow, which may enhance access of compounds, e.g., reactive oxygen species and H_2O_2, that provoke mural remodeling. SHRs have more medial but less adventitial collagen and elastin content than WKY rats (23). Medial thickening over months (22) may mitigate vascular wall stress changes by helping the vessel withstand larger intraluminal systole-diastole pressure vacillations. It cuts medial $L_{p,m+I}$ in both hypertensive rats to approximately half the normotensive $L_{p,m+I}$ with a concomitant $L_{p,t}$ reduction despite increased $L_{p,e+i}$. The unremodeled 2-h FSK-treated aorta has an EC AQP1 increase similar to that of the hypertensive rats but a normotensive $L_{p,m+I}$, resulting in higher $L_{p,t.}$ The chronically hypertensive remodeled, thicker, stiffer, denser, lower $L_{p,m+I}$ media may in themselves lead to endothelial dysfunction, mediated by decreased nitrate/nitrite and prostacyclin and increased endothelin-1 (21).

A variety of hormonal differences distinguish SHR and SD-GB hypertensive rats from their normotensive WKY and SD counterparts. These include an activated sympathetic nervous system with greater blood catecholamine levels, an enhanced renin-angiotensin system (RAS), and elevated plasma arginine vasopressin (AVP) levels [SHRs have up to 4 times the AVP levels of WKY (1, 26, 44, 46, 48, 54, 67)]. All of these eventually enhance endothelial cAMP production by either hormonal, paracrine, or autocrine mechanisms, but each mediator (including angiotensin II, AVP, and catechols) may work through different cellular signalosomes/cellular cascades. Aldosterone, the final product of the RAS pathway, stiffens ECs (38), possibly secondary to the activation of cell membrane ion, e.g., Na^+, channels that colocalize with AQP1 to maintain proper osmolarity (17). The cAMP signaling pathway mediates the major catechols' actions via adenyl cyclase-coupled β-adrenergic receptors that trigger vasorelaxation (53).

The activated SD-GB RAS not only directly affects ECs via angiotensin receptors and aldosterone but also stimulates the hypothalamus to increase pituitary gland AVP production. Angiotensin II activates adenyl cyclase via receptors and a G protein mechanism similar to AVP but likely in a different signalosome. Belkacemi et al. (5) found that AVP causes a fourfold AQP1 upregulation in trophoblasts and that a cAMP analog or a rise in cAMP caused by FSK constitutively upregulates AQP1 expression. AVP increases cAMP via vasopressin type 2 receptors (37, 45) and causes the principal cells of the renal collecting duct to retain water by translocating AQP2 from intracellular storage to the plasma membrane. Although Skowronska et al. (65) found that FSK does not change AQP1 localization in pregnant porcine uterine ECs, short exposure to FSK, to a cAMP analog [Yool et al. (77)], or to AVP [Patil et al. (56)] increases membrane permeability of *Xenopus* oocytes injected with AQP1 cDNA, the latter showing threefold to fourfold increased membrane AQP1 content.

[2] $L_{p,e+i}$ calculation involves *Eq. 1* inverting the small difference of the inverses of $L_{p,t}$ and of $L_{p,m+I}$; small $L_{p,t}$ and $L_{p,e+i}$ errors are magnified in this difference and thus in its inverse's SE.

These studies strongly suggest that a (receptor-mediated if via AVP) cAMP increase rapidly translocates AQP1 to the plasma membrane. Elevated BP likely uses these agonists, e.g., AVP, aldosterone, and adenyl cyclase, to trigger these established EC cAMP AQP1 pathways.

Agonists that contract (hypertensive: catechols, angiotensin II, AVP, etc.) or relax (NO, prostacyclin, endothelium-derived hyperpolarizing factor, etc.) resistance arteries obviously also influence conduit arteries. Shear forces, which vary over the cardiac cycle, profoundly affect EC morphology and function. Hypertension's influence on shear is poorly understood. Laminar shear induces KLF2, which rapidly induces AQP1 and eNOS expression (9, 10) and increases SMC cAMP (14). Human essential hypertension correlates with enhanced KLF2 expression in blood elements (66). Upregulated EC AQP1 can increase NO transport from ECs to medial SMCs (25), which can mitigate SMC proliferation, hypertrophy, and contractility, major factors in vessel wall health. Both the eNOS system and prostanoid responses differ between high-renin hypertensive and normotensive states (6). Instead of enhancing eNOS production of NO from arginine, both high-renin (SHR and SD-GB) and low-renin DOCA hypertensive rats cause it to produce superoxide radicals that enhance NO deactivation (7, 20, 34, 61); blockade of NO degradation leaves cultured aortic ECs from stroke-prone SHRs with NO levels similar to those of WKY rats (20). Although different groups found more (60) or less (12) eNOS, both found lowered eNOS activity in SHR aortic homogenates. This uncoupling of normal eNOS functions interferes with NO's palliative effect on EC quiescence despite increased KLF2 and AQP1; it may be a factor initiating inflammation. In fact, supplying the appropriate biopterin precursors to restore this cofactor can reverse this uncoupling in some disorders and even reverse hypertension (28). The hypertensive aortic SMC is contractile, as in resistance arteries (59), likely because of this faulty response to, e.g., NO and prostacyclin, both of which shift from vasodilatory to vasoconstrictive in hypertensive aortas and to enhanced vasoconstrictor (AVP and angiotensin II) exposure. This implies elevated actin-myosin interaction and increased ATP consumption, which requires increased ATP generation and metabolite efflux; by increasing advection, elevated AQP1 and $L_{p,e+i}$ facilitate these needs. If a feedback system exists between NO formation and KLF2 activation, it might explain elevated KLF2 values in blood elements of hypertensive aortas and enhanced EC AQP1 expression.

Finally, we speculate as to how increased AEC AQP1 may benefit the vessel aside from increased EC NO release. Increased lumen pressure initially increases vessel diameter (then tempered by a myogenic response), which stretches EC junctions. Increased EC AQP1 shifts part of ΔP from acting across the endothelium to acting across the media, thus partially relieving this stress and thickening the SI (33). Increased EC AQP1 may also be mechanically antiatherogenic by enhancing ΔP-driven water transport/$L_{p,t}$ via higher $L_{p,e}$ and fenestral unblocking. Atherosclerosis begins with ΔP-driven advective LDL-cholesterol transport (32, 68) from the blood across extremely rare endothelial leaks (13, 41, 42), associated with low shear and KLF2, into the SI, where LDL can bind to the SI extracellular matrix (15, 64). A decompressed SI shrinks the high-SI LDL leak region by decreasing spot-spreading radial SI pressure gradients (30). Increased transmural water transport ($L_{p,t}$) across the overwhelmingly nonleaky endothelium dilutes local SI LDL concentrations, potentially slowing LDL-extracellular matrix binding kinetics and flushing the SI of unbound LDL (76). The coronary arteries receive mainly diastolic exposure (75), yielding reduced time-average ΔP. By raising the critical ΔP enough to decompress the SI and unblock coronary artery fenestrae, increased AEC AQP1 may be a rapid (hours) response to hypertension, a poorly understood atherosclerosis risk factor, to slow atherogenesis. Media remodeling/thickening that lowers $L_{p,m+I}$ overcomes this effect over months and lowers $L_{p,t}$ to reverse these antiatherogenic trends.

In conclusion, we have shown that the aortas of two strains of hypertensive rats as well as 2-h FSK treatment of aortas from normotensive rats exhibit twofold to threefold upregulation of both their EC AQP1 expression and intimal L_p. All three models have enhanced cAMP; a cAMP mechanism for AQP1 upregulation would be consistent with literature on other systems involving AQP upregulation and trafficking to the plasma membrane. The rapidity of the EC and SMC AQP1 changes suggests that microRNAs may be involved. The pressure dependence of intimal $L_{p,e+i}$ for these cases is consistent with Joshi et al.'s (33) theory that high enough transmural pressure compresses the SI so as to block IEL fenestrae and lower vessel L_p and that a change in the number of functional EC AQP1s shifts the pressure regime over which this compression/L_p drop occurs, possibly unblocking IEL fenestrae in the physiological regime. AQP1 upregulation may be a rapid response to hypertension aimed at enhancing EC NO release to relax vessel wall SMCs and at increasing SI thickness. This increase both relieves EC junction stretch and initially increases transmural water flow, which may be antiatherogenic.

ACKNOWLEDGMENTS

We thank Dr. Mark Arkovitz for teaching us the Goldblatt procedure and Dr. Mark Pezzano for teaching us immunohistochemistry.

GRANTS

We thank the National Heart, Lung, and Blood Institute (Grant 67383) and the National Science Foundation (NSF; Grants IOS-0922051 and CTS-0077520) and PSC-CUNY (ENHC-47-81) for supporting this work. T. Nguyen thanks the Levich Institute Soft Materials NSF-Integrative Graduate Education and Research Traineeship (DGE-0221589), and J. Toussaint thanks the Graduate School and University Center-City University of New York AGEP-0450360 program for partial support.

DISCLOSURES

No conflicts of interest, financial or otherwise, are declared by the authors.

AUTHOR CONTRIBUTIONS

D.S.R. conceived and designed the research with the help of K.-M.J.; J.T., C.B.R., and T.N. performed experiments; J.T., C.B.R., and T.N. performed experiments; J.T., C.B.R., T.N., H.F., S.J., G.W., S.Q., and D.S.R. analyzed data; J.T., C.B.R., T.N., S.Q., K.-M.J., and D.S.R. interpreted results of experiments; J.T., C.B.R., T.N., and S.J. prepared figures; C.B.R. and D.S.R. drafted manuscript; C.B.R., S.Q., and D.S.R. edited and revised manuscript; J.T., C.B.R., T.N., H.F., S.J., G.W., S.Q., K.-M.J., and D.S.R. approved final version of manuscript.

REFERENCES

1. **Bagby SP, McDonald WJ, Mass RD.** Serial renin-angiotensin studies in spontaneously hypertensive and Wistar-Kyoto normotensive rats. Transition from normal- to high-renin status during the established phase of spontaneous hypertension. *Hypertension* 1: 347–354, 1979. doi:10.1161/01.HYP.1.4.347.

2. **Baldwin AL, Wilson LM.** Endothelium increases medial hydraulic conductance of aorta, possibly by release of EDRF. *Am J Physiol Heart Circ Physiol* 264: H26–H32, 1993.
3. **Baldwin AL, Wilson LM, Simon BR.** Effect of pressure on aortic hydraulic conductance. *Arterioscler Thromb* 12: 163–171, 1992. doi:10.1161/01.ATV.12.2.163.
4. **Barakat AI, Uhthoff PAF, Colton CK.** Topographical mapping of sites of enhanced HRP permeability in the normal rabbit aorta. *J Biomech Eng* 114: 283–292, 1992. doi:10.1115/1.2891385.
5. **Belkacemi L, Beall MH, Magee TR, Pourtemour M, Ross MG.** AQP1 gene expression is upregulated by arginine vasopressin and cyclic AMP agonists in trophoblast cells. *Life Sci* 82: 1272–1280, 2008. doi:10.1016/j.lfs.2008.04.014.
6. **Bernatova I.** Endothelial dysfunction in experimental models of arterial hypertension: cause or consequence? *BioMed Res Int* 2014: 598271, 2014. doi:10.1155/2014/598271.
7. **Bhatia J, Tabassum F, Sharma AK, Bharti S, Golechha M, Joshi S, Sayeed Akhatar M, Srivastava AK, Arya DS.** Emblica officinalis exerts antihypertensive effect in a rat model of DOCA-salt-induced hypertension: role of (p) eNOS, NO and oxidative stress. *Cardiovasc Toxicol* 11: 272–279, 2011. doi:10.1007/s12012-011-9122-2.
8. **Blanc L, Liu J, Vidal M, Chasis JA, An X, Mohandas N.** The water channel aquaporin-1 partitions into exosomes during reticulocyte maturation: implication for the regulation of cell volume. *Blood* 114: 3928–3934, 2009. doi:10.1182/blood-2009-06-230086.
9. **Boon RA, Hergenreider E, Dimmeler S.** Atheroprotective mechanisms of shear stress-regulated microRNAs. *Thromb Haemost* 108: 616–620, 2012. doi:10.1160/TH12-07-0491.
10. **Boon RA, Leyen TA, Fontijn RD, Fledderus JO, Baggen JM, Volger OL, van Nieuw Amerongen GP, Horrevoets AJ.** KLF2-induced actin shear fibers control both alignment to flow and JNK signaling in vascular endothelium. *Blood* 115: 2533–2542, 2010. doi:10.1182/blood-2009-06-228726.
11. **Caro CG, Fitz-Gerald JM, Schroter RC.** Atheroma and arterial wall shear. Observation, correlation and proposal of a shear dependent mass transfer mechanism for atherogenesis. *Proc R Soc Lond B Biol Sci* 177: 109–159, 1971. doi:10.1098/rspb.1971.0019.
12. **Chou TC, Yen MH, Li CY, Ding YA.** Alterations of nitric oxide synthase expression with aging and hypertension in rats. *Hypertension* 31: 643–648, 1998. doi:10.1161/01.HYP.31.2.643.
13. **Chuang PT, Cheng HJ, Lin SJ, Jan KM, Lee MM, Chien S.** Macromolecular transport across arterial and venous endothelium in rats. Studies with Evans blue-albumin and horseradish peroxidase. *Arteriosclerosis* 10: 188–197, 1990. doi:10.1161/01.ATV.10.2.188.
14. **Dubey RK, Gillespie DG, Mi Z, Rosselli M, Keller PJ, Jackson EK.** Estradiol inhibits smooth muscle cell growth in part by activating the cAMP-adenosine pathway. *Hypertension* 35: 262–266, 2000. doi:10.1161/01.HYP.35.1.262.
15. **Frank JS, Fogelman AM.** Ultrastructure of the intima in WHHL and cholesterol-fed rabbit aortas prepared by ultra-rapid freezing and freeze-etching. *J Lipid Res* 30: 967–978, 1989.
16. **Gadau J, Peters H, Kastner C, Kühn H, Nieminen-Kelhä M, Khadzhynov D, Krämer S, Castrop H, Bachmann S, Theilig F.** Mechanisms of tubular volume retention in immune-mediated glomerulonephritis. *Kidney Int* 75: 699–710, 2009. doi:10.1038/ki.2008.649.
17. **Gao C, Tang J, Li R, Huan J.** Specific inhibition of AQP1 water channels in human pulmonary microvascular endothelial cells by small interfering RNAs. *J Trauma Acute Care Surg* 72: 150–161, 2012. doi:10.1097/TA.0b013e318230e25d.
18. **Giannakoulas G, Giannoglou G, Soulis J, Farmakis T, Papadopoulou S, Parcharidis G, Louridas G.** A computational model to predict aortic wall stresses in patients with systolic arterial hypertension. *Med Hypotheses* 65: 1191–1195, 2005. doi:10.1016/j.mehy.2005.06.017.
19. **Goldblatt H, Lynch J, Hanzal RF, Summerville WW.** Studies on experimental hypertension. 1. The production of persistent elevation of systolic blood pressure by means of renal ischemia. *J Exp Med* 59: 347–379, 1934. doi:10.1084/jem.59.3.347.
20. **Grunfeld S, Hamilton CA, Mesaros S, McClain SW, Dominiczak AF, Bohr DF, Malinski T.** Role of superoxide in the depressed nitric oxide production by the endothelium of genetically hypertensive rats. *Hypertension* 26: 854–857, 1995. doi:10.1161/01.HYP.26.6.854.
21. **Guo X, Lu X, Yang J, Kassab GS.** Increased aortic stiffness elevates pulse and mean pressure and compromises endothelial function in Wistar rats. *Am J Physiol Heart Circ Physiol* 307: H880–H887, 2014. doi:10.1152/ajpheart.00265.2014.
22. **Hadjiisky P, Peyri N, Grosgogeat Y.** Tunica media changes in the spontaneously hypertensive rat (SHR). *Atherosclerosis* 65: 125–137, 1987. doi:10.1016/0021-9150(87)90014-1.
23. **Han WQ, Wu LY, Zhou HY, Zhang J, Che ZQ, Wu YJ, Liu JJ, Zhu DL, Gao PJ.** Changes in the composition of the thoracic aortic wall in spontaneously hypertensive rats treated with losartan or spironolactone. *Clin Exp Pharmacol Physiol* 36: 583–588, 2009. doi:10.1111/j.1440-1681.2008.05116.x.
24. **Herrera M, Garvin JL.** Aquaporins as gas channels. *Pflugers Arch* 462: 623–630, 2011. doi:10.1007/s00424-011-1002-x.
25. **Herrera M, Hong NJ, Garvin JL.** Aquaporin-1 transports NO across cell membranes. *Hypertension* 48: 157–164, 2006. doi:10.1161/01.HYP.0000223652.29338.77.
26. **Hirata Y, Matsuoka H, Hayakawa H, Sugimoto T, Suzuki E, Sugimoto T, Kangawa K, Matsuo H.** Role of endogenous atrial natriuretic peptide in regulating sodium excretion in spontaneously hypertensive rats. Effects of neutral endopeptidase inhibition. *Hypertension* 17: 1025–1032, 1991. doi:10.1161/01.HYP.17.6.1025.
27. **Homma S, Ishii T, Tsugane S, Hirose N.** Different effects of hypertension and hypercholesterolemia on the natural history of aortic atherosclerosis by the stage of intimal lesions. *Atherosclerosis* 128: 85–95, 1997. doi:10.1016/S0021-9150(96)05970-9.
28. **Hong HJ, Hsiao G, Cheng TH, Yen MH.** Supplemention with tetrahydrobiopterin suppresses the development of hypertension in spontaneously hypertensive rats. *Hypertension* 38: 1044–1048, 2001. doi:10.1161/hy1101.095331.
29. **Huang Y, Jan K-M, Rumschitzki D, Weinbaum S.** Structural changes in rat aortic intima due to transmural pressure. *J Biomech Eng* 120: 476–483, 1998. doi:10.1115/1.2798017.
30. **Huang Y, Rumschitzki D, Chien S, Weinbaum S.** A fiber matrix model for the filtration through fenestral pores in a compressible arterial intima. *Am J Physiol Heart Circ Physiol* 272: H2023–H2039, 1997.
32. **Huang Y, Rumschitzki D, Chien S, Weinbaum S.** A fiber matrix model for the growth of macromolecular leakage spots in the arterial intima. *J Biomech Eng* 116: 430–445, 1994. doi:10.1115/1.2895794.
33. **Joshi S, Jan KM, Rumschitzki DS.** Aquaporin-1 shifts the critical transmural pressure to compress the aortic intima and change transmural flow: theory and implications. *Am J Physiol Heart Circ Physiol* 309: H1974–H1986, 2015. doi:10.1152/ajpheart.00316.2015.
34. **Jung O, Schreiber JG, Geiger H, Pedrazzini T, Busse R, Brandes RP.** gp91phox-containing NADPH oxidase mediates endothelial dysfunction in renovascular hypertension. *Circulation* 109: 1795–1801, 2004. doi:10.1161/01.CIR.0000124223.00113.A4.
35. **Kass M, Witkin A, Terzopoulos D.** Snakes: active contour models. *Int J Comput Vis* 1: 321–331, 1998. doi:10.1007/BF00133570.
36. **Kastner C, Pohl M, Sendeski M, Stange G, Wagner CA, Jensen B, Patzak A, Bachmann S, Theilig F.** Effects of receptor-mediated endocytosis and tubular protein composition on volume retention in experimental glomerulonephritis. *Am J Physiol Renal Physiol* 296: F902–F911, 2009. doi:10.1152/ajprenal.90451.2008.
37. **Kaufmann JE, Oksche A, Wollheim CB, Günther G, Rosenthal W, Vischer UM.** Vasopressin-induced von Willebrand factor secretion from endothelial cells involves V2 receptors and cAMP. *J Clin Invest* 106: 107–116, 2000. doi:10.1172/JCI9516.
38. **Kliche K, Jeggle P, Pavenstädt H, Oberleithner H.** Role of cellular mechanics in the function and life span of vascular endothelium. *Pflugers Arch* 462: 209–217, 2011. doi:10.1007/s00424-011-0929-2.
39. **Lee J, Kim S, Kim J, Jeong MH, Oh Y, Choi KC.** Increased expression of renal aquaporin water channels in spontaneously hypertensive rats. *Kidney Blood Press Res* 29: 18–23, 2006. doi:10.1159/000092483.
40. **Lee MY, Wu CM, Yu KH, Chu CS, Lee KT, Sheu SH, Lai WT.** Association between wall shear stress and carotid atherosclerosis in patients with never treated essential hypertension. *Am J Hypertens* 22: 705–710, 2009. doi:10.1038/ajh.2009.77.
41. **Lin SJ, Jan KM, Weinbaum S, Chien S.** Transendothelial transport of low density lipoprotein in association with cell mitosis in rat aorta. *Arteriosclerosis* 9: 230–236, 1989. doi:10.1161/01.ATV.9.2.230.
42. **Lin SJ, Jan KM, Chien S.** Role of dying endothelial cells in transendothelial macromolecular transport. *Arteriosclerosis* 10: 703–709, 1990. doi:10.1161/01.ATV.10.5.703.
43. **Ma SK, Bae EH, Kim IJ, Choi C, Lee J, Kim SW.** Altered renal expression of aquaporin water channels and sodium transporters in rats

with two-kidney, one-clip hypertension. *Kidney Blood Press Res* 32: 411–420, 2009. doi:10.1159/000264232.
44. **Martinez-Maldonado M.** Pathophysiology of renovascular hypertension. *Hypertension* 17: 707–719, 1991. doi:10.1161/01.HYP.17.5.707.
45. **Méchaly I, Laurent F, Portet K, Serrano J, Cros G.** Vasopressin V2 (SR121463A) and V1a (SR49059) receptor antagonists both inhibit desmopressin vasorelaxing activity. *Eur J Pharmacol* 383: 287–290, 1999. doi:10.1016/S0014-2999(99)00641-X.
46. **Möhring J, Kintz J, Schoun J.** Studies on the role of vasopressin in blood pressure control of spontaneously hypertensive rats with established hypertension (SHR, stroke-prone strain). *J Cardiovasc Pharmacol* 1: 593–608, 1979. doi:10.1097/00005344-197911000-00001.
47. **Montiel V, Leon Gomez E, Bouzin C, Esfahani H, Romero Perez M, Lobysheva I, Devuyst O, Dessy C, Balligand JL.** Genetic deletion of aquaporin-1 results in microcardia and low blood pressure in mouse with intact nitric oxide-dependent relaxation, but enhanced prostanoids-dependent relaxation. *Pflugers Arch* 466: 237–251, 2014. doi:10.1007/s00424-013-1325-x.
48. **Morris M, Keller M, Sundberg DK.** Changes in paraventricular vasopressin and oxytocin during the development of spontaneous hypertension. *Hypertension* 5: 476–481, 1983. doi:10.1161/01.HYP.5.4.476.
49. **Murphy WR, Coleman TG, Smith TL, Stanek KA.** Effects of graded renal artery constriction on blood pressure, renal artery pressure, and plasma renin activity in Goldblatt hypertension. *Hypertension* 6: 68–74, 1984. doi:10.1161/01.HYP.6.1.68.
50. **Nerem RM.** Hemodynamics and the vascular endothelium. *J Biomech Eng* 115, *4B*: 510–514, 1993. doi:10.1115/1.2895532.
51. **Nerem RM, Harrison DG, Taylor WR, Alexander RW.** Hemodynamics and vascular endothelial biology. *J Cardiovasc Pharmacol* 21, *Suppl* 1: S6–S10, 1993. doi:10.1097/00005344-199321001-00002.
52. **Nguyen T, Toussaint J, Xue Y, Raval C, Cancel L, Russell S, Shou Y, Sedes O, Sun Y, Yakobov R, Tarbell JM, Jan KM, Rumschitzki DS.** Aquaporin-1 facilitates pressure-driven water flow across the aortic endothelium. *Am J Physiol Heart Circ Physiol* 308: H1051–H1064, 2015. doi:10.1152/ajpheart.00499.2014.
53. **Orlov SN, Tremblay J, Hamet P.** cAMP signaling inhibits dihydropyridine-sensitive Ca^{2+} influx in vascular smooth muscle cells. *Hypertension* 27: 774–780, 1996. doi:10.1161/01.HYP.27.3.774.
54. **Pacák K, Yadid G, Jakab G, Lenders JW, Kopin IJ, Goldstein DS.** In vivo hypothalamic release and synthesis of catecholamines in spontaneously hypertensive rats. *Hypertension* 22: 467–478, 1993. doi:10.1161/01.HYP.22.4.467.
55. **Pacher P, Beckman JS, Liaudet L.** Nitric oxide and peroxynitrite in health and disease. *Physiol Rev* 87: 315–424, 2007. doi:10.1152/physrev.00029.2006.
56. **Patil RV, Han Z, Wax MB.** Regulation of water channel activity of aquaporin 1 by arginine vasopressin and atrial natriuretic peptide. *Biochem Biophys Res Commun* 238: 392–396, 1997. doi:10.1006/bbrc.1997.7310.
57. **Postaire O, Tournaire-Roux C, Grondin A, Boursiac Y, Morillon R, Schäffner AR, Maurel C.** A PIP1 aquaporin contributes to hydrostatic pressure-induced water transport in both the root and rosette of Arabidopsis. *Plant Physiol* 152: 1418–1430, 2010. doi:10.1104/pp.109.145326.
58. **Presnell JK, Schreibman MP.** *Humason's Animal Tissue Techniques*. Baltimore, MD: Johns Hopkins University Press, 1979.
59. **Risler NR, Cruzado MC, Miatello RM.** Vascular remodeling in experimental hypertension. *Sci World J* 5: 959–971, 2005. doi:10.1100/tsw.2005.122.
60. **Sánchez M, Galisteo M, Vera R, Villar IC, Zarzuelo A, Tamargo J, Pérez-Vizcaíno F, Duarte J.** Quercetin downregulates NADPH oxidase, increases eNOS activity and prevents endothelial dysfunction in spontaneously hypertensive rats. *J Hypertens* 24: 75–84, 2006. doi:10.1097/01.hjh.0000198029.22472.d9.
61. **Schnackenberg CG, Welch WJ, Wilcox CS.** Normalization of blood pressure and renal vascular resistance in SHR with a membrane-permeable superoxide dismutase mimetic: role of nitric oxide. *Hypertension* 32: 59–64, 1998. doi:10.1161/01.HYP.32.1.59.
62. **Shanahan CM, Connolly DL, Tyson KL, Cary NR, Osbourn JK, Agre P, Weissberg PL.** Aquaporin-1 is expressed by vascular smooth muscle cells and mediates rapid water transport across vascular cell membranes. *J Vasc Res* 36: 353–362, 1999. doi:10.1159/000025674.
63. **Shou Y, Jan KM, Rumschitzki DS.** Transport in rat vessel walls. I. Hydraulic conductivities of the aorta, pulmonary artery, and inferior vena cava with intact and denuded endothelia. *Am J Physiol Heart Circ Physiol* 291: H2758–H2771, 2006. doi:10.1152/ajpheart.00610.2005.
64. **Simionescu N, Vasile E, Lupu F, Popescu G, Simionescu M.** Prelesional events in atherogenesis. Accumulation of extracellular cholesterol-rich liposomes in the arterial intima and cardiac valves of the hyperlipidemic rabbit. *Am J Pathol* 123: 109–125, 1986.
65. **Skowronska A, Mlotkowska P, Okrasa S, Nielsen S, Skowronski MT.** Modulatory effects of steroid hormones, oxytocin, arachidonic acid, forskolin and cyclic AMP on the expression of aquaporin 1 and aquaporin 5 in the porcine uterus during placentation. *J Physiol Pharmacol* 67: 311–319, 2016.
66. **Stoynev N, Dimova I, Rukova B, Hadjidekova S, Nikolova D, Toncheva D, Tankova T.** Gene expression in peripheral blood of patients with hypertension and patients with type 2 diabetes. *J Cardiovasc Med (Hagerstown)* 15: 702–709, 2014. doi:10.2459/JCM.0b013e32835dbcc8.
67. **Takiyyuddin MA, De Nicola L, Gabbai FB, Dinh TQ, Kennedy B, Ziegler MG, Sabban EL, Parmer RJ, O'Connor DT.** Catecholamine secretory vesicles. Augmented chromogranins and amines in secondary hypertension. *Hypertension* 21: 674–679, 1993. doi:10.1161/01.HYP.21.5.674.
68. **Tedgui A, Lever MJ.** The interaction of convection and diffusion in the transport of ^{131}I-albumin within the media of the rabbit thoracic aorta. *Circ Res* 57: 856–863, 1985. doi:10.1161/01.RES.57.6.856.
69. **Tedgui A, Lever MJ.** Filtration through damaged and undamaged rabbit thoracic aorta. *Am J Physiol Heart Circ Physiol* 247: H784–H791, 1984.
70. **Tomassoni D, Bramanti V, Amenta F.** Expression of aquaporins 1 and 4 in the brain of spontaneously hypertensive rats. *Brain Res* 1325: 155–163, 2010. doi:10.1016/j.brainres.2010.02.023.
71. **Vargas CB, Vargas FF, Pribyl JG, Blackshear PL.** Hydraulic conductivity of the endothelial and outer layers of the rabbit aorta. *Am J Physiol Heart Circ Physiol* 236: H53–H60, 1979.
72. **Vlad M, Bordas E, Caseanu E, Uza G, Creteanu E, Polinicenco C.** Effect of cuprofilin on experimental atherosclerosis. *Biol Trace Elem Res* 48: 99–109, 1995. doi:10.1007/BF02789082.
73. **Vlad M, Uza G, Zirbo M, Olteanu D.** Free radicals, ceruloplasmin, and copper concentration in serum and aortic tissue in experimental atherosclerosis. *Nutrition* 11, *Suppl*: 588–591, 1995.
74. **Weinberg PD.** Disease patterns at arterial branches and their relation to flow. *Biorheology* 39: 533–537, 2002.
75. **Westerhof N, Boer C, Lamberts RR, Sipkema P.** Cross-talk between cardiac muscle and coronary vasculature. *Physiol Rev* 86: 1263–1308, 2006. doi:10.1152/physrev.00029.2005.
76. **Yin Y, Lim K-H, Weinbaum S, Chien S, Rumschitzki DS.** A model for the initiation and growth of extracellular lipid liposomes in arterial intima. *Am J Physiol Heart Circ Physiol* 272: H1033–H1046, 1997.
77. **Yool AJ, Stamer WD, Regan JW.** Forskolin stimulation of water and cation permeability in aquaporin 1 water channels. *Science* 273: 1216–1218, 1996. doi:10.1126/science.273.5279.1216.